Empirical Relationships for Estimating Liquid Water Fraction of Melting Snowflakes

RYOHEI MISUMI

National Research Institute for Earth Science and Disaster Prevention, Tsukuba, Japan

HIROKI MOTOYOSHI, SATORU YAMAGUCHI, SENTO NAKAI, AND MASAAKI ISHIZAKA

Snow and Ice Research Center, National Research Institute for Earth Science and Disaster Prevention, Nagaoka, Japan

YASUSHI FUJIYOSHI

Institute of Low Temperature Science, Hokkaido University, Sapporo, Japan

(Manuscript received 17 May 2013, in final form 26 July 2014)

ABSTRACT

The liquid water fraction of individual snowflakes f is an important parameter when calculating the radar reflectivity of a melting layer. A ground-based observation of f at Nagaoka, Japan, was conducted by using dye-treated filter papers that were kept at a temperature of 0°C. From the results of these measurements, which consisted of 6179 particles taken with 44 sheets of filter paper, two empirical relationships are proposed. The first is a relationship between the ratio of liquid water flux to total precipitation intensity (F_L; taking values from 0 to 1) and meteorological surface data. The second is a relationship to estimate f using the melted diameter of a snowflake, median mass diameter, and F_L. It was determined that the root-mean-square errors for estimating F_L and f by using these relationships were 0.160 and 0.144, respectively. It was also found that the ratio of raindrop flux to the total precipitation intensity F_R was always below 0.1 when F_L was less than 0.6 but increased rapidly when F_L exceeded 0.8.

1. Introduction

When snowflakes fall through a melting layer, high radar reflectivity occurs and a bright band can be observed. Bright bands are caused by changes in the dielectric constant of snowflakes as a result of melting, activation of aggregation, and a decrease in the number density of hydrometeors because of the increase of fall velocity (Austin and Bemis 1950). Because the changes in dielectric constant and fall velocity are related to the melted fraction of hydrometeors (e.g., Klaassen 1988; Szyrmer and Zawadzki 1999; Zawadzki et al. 2005), observing and modeling the liquid water fraction of snowflakes is important. In this study, the liquid water fraction f of a snowflake is defined by the ratio of the mass of liquid water M_w contained in the snowflake to the mass of the snowflake M_s as follows:

$$f = M_w/M_s. \quad (1)$$

Previous observational and experimental studies of melting snowflakes suggest that melted water penetrates to the inside of aggregates (Matsuo and Sasyo 1981; Mitra et al. 1990) or accumulates at the intersection of branches (Knight 1979; Fujiyoshi 1986; Oraltay and Hallett 1989, 2005). In either case, the majority of melted water falls with the solid part of the snowflake, and some of the melted water sheds away under certain conditions (Oraltay and Hallett 1989). Sufficient observational data have not been obtained for the amount of liquid water in snowflakes, however, since an observation technique has not been well established.

Nakamura (1960) made the first attempt to measure the liquid water fraction of snowflakes. By using a dye-treated filter paper to collect falling snowflakes, he measured the area A_1 of the spot produced after a snowflake has fallen onto the paper and the area A_2 after the snowflake has completely melted. Then, he calculated the liquid water fraction as A_1/A_2. There are two problems when using this method, however. One is that melting or freezing can occur on the filter paper unless

Corresponding author address: Ryohei Misumi, National Research Institute for Earth Science and Disaster Prevention, 3-1 Tennodai, Tsukba 305-0006, Japan.
E-mail: misumi@bosai.go.jp

DOI: 10.1175/JAMC-D-13-0169.1

the papers are maintained at exactly 0°C. The other problem is that the melted water does not always completely soak into the filter paper when a snowflake has a three-dimensional structure. The latter problem could cause underestimation of the liquid water fraction. Sasyo et al. (1991) developed an instrument to collect snowflakes on filter papers that are kept at 0°C by a cooling unit, but the second problem was not solved. To the best of our knowledge, there have been no further studies on the measurement of the liquid water fraction of individual snowflakes.

In this study, a calibration was conducted that utilized imitation snowflakes to overcome the underestimation problem of the previous technique mentioned above. As a result, the liquid water fraction of melting snowflakes was measured more accurately than in previous studies. On the basis of the results of our measurements, which consisted of 6179 particles (3632 melting snowflakes and 2547 raindrops) taken with 44 sheets of filter paper, we propose empirical relationships to estimate the contribution of the liquid water flux to the precipitation intensity and to estimate the liquid water fraction of individual snowflakes.

2. Observation

a. Instrument

The instrument used in this study (Fig. 1) was developed by Sasyo et al. (1991) and manufactured by Suga Test Instrument Co., Ltd. The instrument has inlets that open for 10 s to collect falling snowflakes on a dye-treated filter paper. The area of the filter paper is 430 cm^2. Then, a motor rolls the filter paper and moves it to a cooling unit that keeps it at a temperature of 0°C. After 120 s, when the liquid water has soaked into the filter paper, the cooling unit moves away, and an image of the spots is taken by a camera beneath the paper. Next, a warming unit is placed under the filter paper to melt the snowflakes completely. Then, the warming unit moves away, and another image of the spots is taken. This cycle is repeated automatically at 10-min intervals.

The images of the spots are analyzed with ImageJ software that was developed by the National Institutes of Health of the United States. The images of the spots on the filter paper (Fig. 2a) are converted into binary images, and any noise is removed (Fig. 2b). By using the command ''analyze particles'' in ImageJ, spots are labeled and their areas are measured (Fig. 2c). The relationship between the area of spots and the mass of water was established by a laboratory experiment (Fig. 3). From the best-fit curve of the 24 data, the relationship between the area of a spot S (cm^2) and the mass of water M (g) was obtained as the following equation:

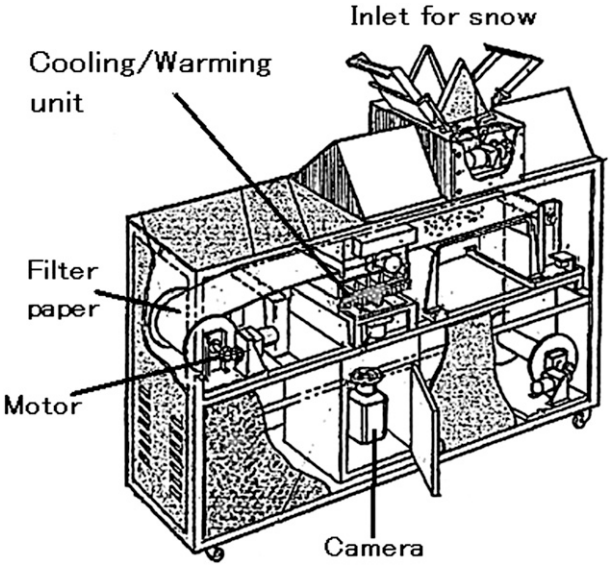

FIG. 1. The instrument used in this study.

$$M = 5.91 \times 10^{-3} S^{1.12}. \quad (2)$$

When using (2) to estimate M, the standard deviation of the relative errors was 6.6%. For the observations, the areas of the spots on the filter papers were converted into water mass using (2). The liquid water fraction f_1 of a snowflake was calculated as follows:

$$f_1 = M_1/M_2, \quad (3)$$

where M_1 is the mass of the liquid water soaked into the filter paper after a snowflake has fallen onto the paper and M_2 is the mass of the snowflake.

b. Calibration

For calibration of the measurement process in this study, imitation snowflakes were used so that the amount of soaked water could be measured accurately. The imitation snowflakes were made from a sponge of polyurethane (Fig. 4a) that was cut to determine their size–mass relationship, which is similar to that of the lightly rimed snowflakes observed by Ishizaka (1995) (Fig. 4b). For the calibration, the polyurethane represents the ice skeleton of a melting snowflake. Because the empirical line of Ishizaka (1995) represents the size–mass relationship of weakly rimed snowflakes around the observation area of the current study (Nagaoka, Japan), it was used during the production of imitation snowflakes. The density of the polyurethane used in this study (1.017 g cm^{-3}) was close to that of ice (0.917 g cm^{-3}).

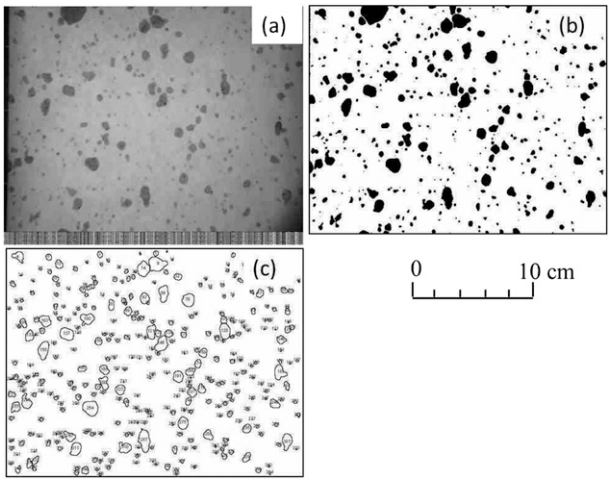

FIG. 2. (a) Photograph of spots on a filter paper. (b) Binary image of the spots. (c) Spots labeled by ImageJ.

A total of 48 imitation snowflakes were prepared for the calibration.

The calibration was conducted in two steps. In the first step, the dry weights of the imitation snowflakes were measured with an electronic balance (Shimadzu model AUW120; resolution of 0.1 mg). Then, liquid water was placed onto the snowflakes, and the snowflakes were then dropped from a height of 80 cm onto a dye-treated filter paper. After the total weight of the filter paper and wet snowflake was measured, the mass of liquid water was calculated by subtracting the weight of the dry snowflake and the filter paper. In this way, accurate values were obtained for the liquid water fraction f of imitation snowflakes. In the second step, the area of the spots on the filter paper was converted into the mass of water using (2), and the liquid water fraction f_1 was estimated. Figure 4c shows a comparison between f and f_1. By evaluating the best-fit curve, the correction line for the values of f_1 observed with filter paper was obtained as

$$f = f_1^{0.403}, \tag{4}$$

where f is the liquid water fraction measured by the electronic balance. According to the correction line, values were underestimated when the filter-paper method was used. Moreover, data are scattered around the best-fit curve. The root-mean-square error (RMSE) of the best-fit curve was estimated to be 0.108.

There are problems with the calibration when imitation snowflakes are used. First, the mesh structure of a snowflake never collapses because of melting. Even when the liquid water fraction is very large, liquid water is kept within the structure of the polyurethane. This situation reduces the amount of liquid water that can be soaked into the filter paper. Another problem is that the wettability of polyurethane is different from that of ice. This would also affect the amount of water that is transferred from a snowflake to a filter paper. It is very difficult to evaluate the calibration errors caused by these factors. Therefore, another experiment was conducted that utilizes natural snow to validate the calibration. Natural snow was collected during the winter and stored in a freezer room. According to a microscope observation, the natural snowflakes maintained their branchlike structures (images not shown). In a low-temperature (−5°C) room, several grams of the natural snow was placed into a dish, and the dry weight was measured. Then, nonfreezing liquid (10% solution of ethylene glycol) was added to the snow, and the mixture was gently stirred with a plastic stick. The weight of this mixture was then measured. In this way, the bulk liquid water fraction was obtained for "wet snow." Next, tweezers were used to drop several snow particles in the mixture onto dye-treated filter papers. Because the nonfreezing liquid was contained inside the structure of the snow and was not uniformly mixed with snow, the liquid water fraction of these individually dropped snow particles differed from the bulk value. Thus, a comparison was made between the mass-weighted mean liquid water fraction of several snow particles measured with the filter papers and the bulk value of the liquid water fraction. This experiment was repeated 16 times (Fig. 5). The values obtained by the filter-paper measurements were consistently lower than the bulk liquid water fraction (white circles in Fig. 5). When these values were corrected with (4), the RMSE decreased from 0.267 to 0.130 (black circles in Fig. 5). These results support the effectiveness of the calibration. Equation (4) was used to correct all of the values observed with the filter-paper method.

c. *Observation site*

Observations were conducted at the Snow and Ice Research Center in Nagaoka (37.4259°N, 138.8867°E), where snowfall frequently occurs just above 0°C (Yamaguchi et al. 2013). The instrument shown in Fig. 1 was enclosed by a wind protection net. Temperature T and relative humidity RH were obtained using a thermometer (Ota Keiki model OW-1–1; accuracy of ±0.15°C) and a humidity sensor [Vaisala, Inc., HUMICAP 180; accuracy of ±(1.0 + 0.008RH)%], respectively, and observations were conducted at 1-min intervals. A vertical-pointing K-band radar [Meteorologische Messtechnik GmbH (METEK) Micro Rain Radar] was also used to obtain vertical profiles of radar reflectivity at 50-m intervals from 50 to 1550 m above ground level. The spectral reflectivity derived from the radar was converted into an

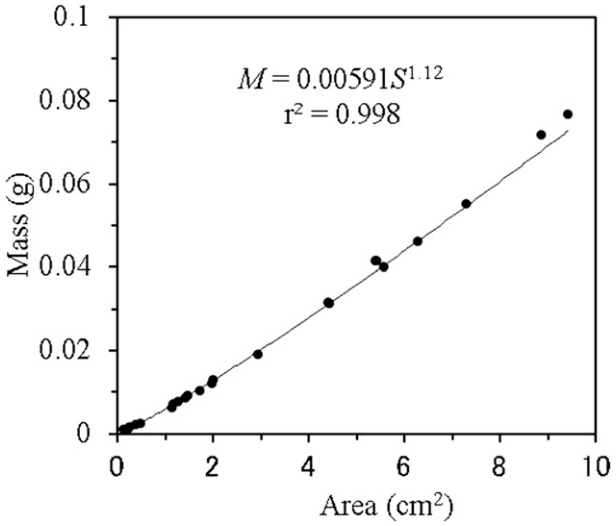

FIG. 3. Relationship between the area of spots S and the mass of water M; r^2 indicates the coefficient of determination.

equivalent radar reflectivity factor Z_e by the method of Maahn and Kollias (2012) as

$$Z_e = 10^{18}\frac{\lambda^4}{\pi^5}|K|^2\int \eta(v)\,dv, \tag{5}$$

where λ is the wavelength of the radar (m), $|K|^2$ is the dielectric factor for water, v is the Doppler velocity (m s^{-1}), and η is the spectral reflectivity (s m^{-2}).

Data were sampled on 26 March 2011; 9, 22, 23, and 24 December 2011; and 12 March 2012. A total of 6179 precipitating particles were measured using 44 sheets of filter paper. The types of the snow particles were identified simultaneously with a microscope. Most of the snowflakes were rimed aggregates composed of plates with dendritic or sectorlike extensions. Although graupel was sometimes sampled, their data were not analyzed because the focus of this study is on snowflakes. Snowflakes in melting stages 1–5 of the classification scheme of Fujiyoshi (1986) and raindrops were observed to sometimes fall simultaneously. Sometimes very small dry particles with $f = 0$ were found, but they were excluded from the analysis because they are considered to be splinters produced by the collisions between snowflakes and the filter paper. The breakup of wet snowflakes seemed to be rare, probably because they were bonded with liquid water.

For convenience, the contribution F_L of liquid water flux (i.e., the flux of raindrops and liquid water contained in snowflakes) to precipitation intensity is defined as follows:

$$F_L = R_L/R, \tag{6}$$

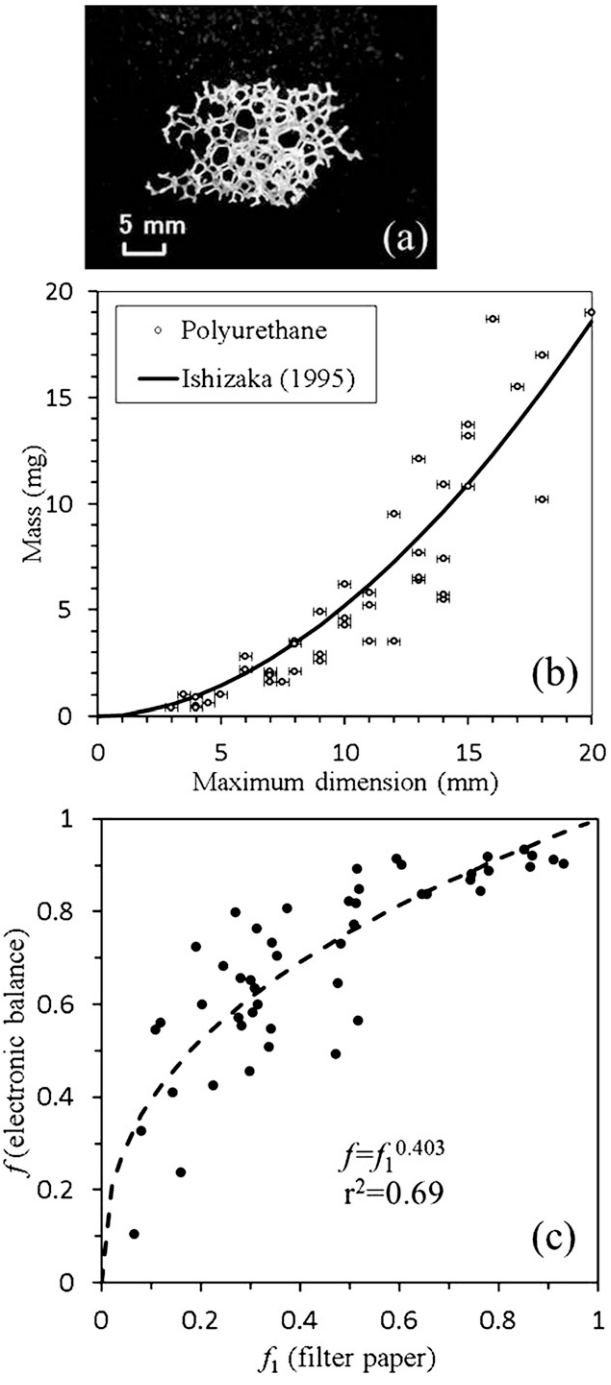

FIG. 4. (a) Image of an imitation snowflake used for calibration. (b) Relationship between maximum dimension and the mass of the imitation snowflakes (circles) and that of lightly rimed aggregates observed by Ishizaka (1995) (solid line). Error bars indicate the range of measurement errors. (c) Relationship between the mass fraction of liquid water of the imitation snowflakes observed by filter papers and that measured by an electronic balance. The dashed line represents the best-fit curve, and the coefficient of determination is indicated by r^2.

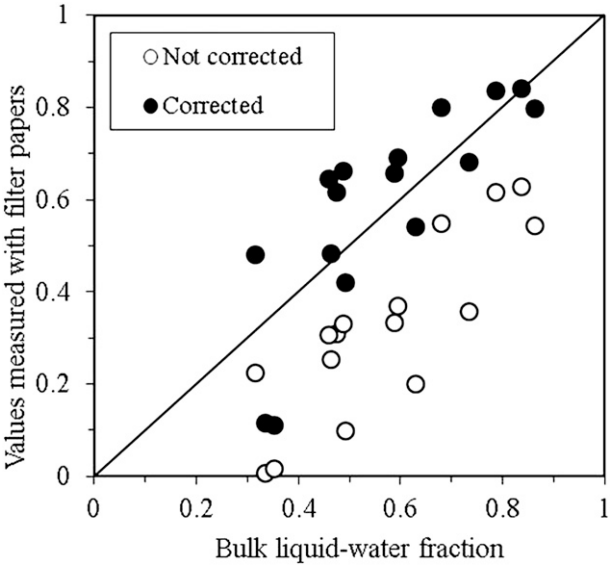

FIG. 5. Relationship between the bulk liquid water fraction of natural snow and the mass-weighted mean liquid water fraction measured with filter paper. Open circles are the measured values, and filled circles are the values corrected using (4).

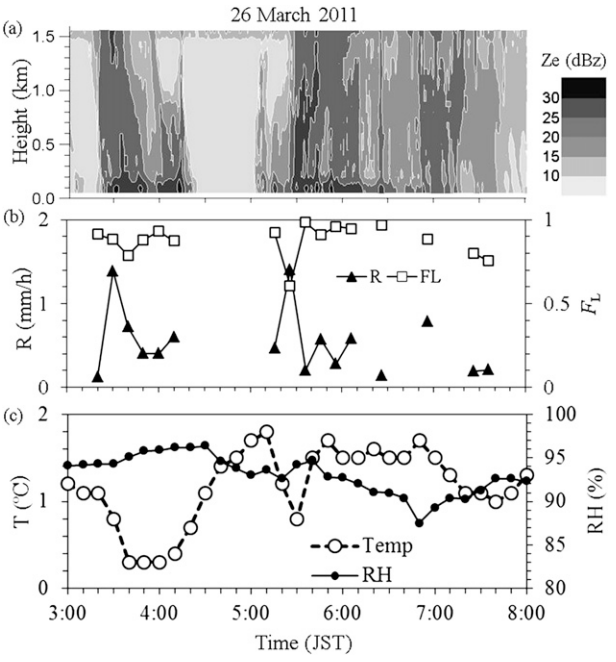

FIG. 6. Time variation of (a) a vertical profile of Z_e observed by a K-band vertical-pointing radar, (b) rainfall intensity R and F_L, and (c) T and RH at the surface from 0300 to 0800 JST 26 Mar 2011.

where R and R_L are total precipitation intensity and the intensity of liquid water, respectively; R (R_L) was obtained as the total mass of the precipitating particles (the total mass of liquid water) on a filter paper divided by the exposure time and area.

In this observation, raindrops can be distinguished from melting snowflakes because raindrops are at $f = 1.0$. The contribution of raindrop flux to total precipitation intensity is also important information in radar meteorology and is defined as

$$F_R = R_R/R, \tag{7}$$

where R_R is the precipitation intensity of raindrops, which is obtained as the total mass of raindrops on a filter paper divided by the exposure time and area.

3. Results

a. Description of events

We first briefly describe the events that were observed in this study. On 26 March 2011 (Fig. 6), melting snowflakes were observed after 0300 Japan standard time (JST; UTC + 9 h) in association with the passage of a mesoscale depression. Figure 6 shows the time variation of R, F_L, T, and RH and a vertical profile of Z_e. The large values of Z_e near the surface indicate a bright band (Fig. 6a). During the period of this bright band, F_L was maintained above 0.8, except at 0526 JST when a rapid decrease of T and F_L occurred. After 0630 JST, the bright band became unclear, and F_L gradually decreased.

On 9 December 2011 (Fig. 7), continuous precipitation was observed in association with the passage of a mesoscale depression. The precipitation type changed from rainfall to melting snow after 1500 JST, when the temperature decreased from 2° to 0.2°C (Fig. 7c). After 1600 JST, the temperature remained between 0° and 0.5°C. The F_L had a tendency to decrease in accordance with the decrease in temperature, but, for the most part, the values fluctuated (Fig. 7b). A bright band was observed near the ground for a short period between 1500 and 1600 JST (Fig. 7a). The missing R and F_L data after 1800 JST were due to the removal of graupel data.

From 22 to 23 December 2011, snowfall was observed with temperatures between 0° and 3°C, but the majority of the hydrometeors were graupel (figure not shown). The data from 2342 JST 22 December to 0011 JST 23 December were used for the analysis in which melting snowflakes were observed. On 24 December 2011, melting snowflakes were observed in the afternoon when the temperature increased. Because of troubles with the instrument, however, only four sheets of filter paper were used that day. On 12 March 2012, the precipitation type mainly consisted of graupel, and melting snowflakes were only observed for a very short time. The data for 0913 and 1214 JST on that day were utilized.

b. *Contribution of liquid water flux to precipitation intensity*

Before discussing the liquid water fraction of individual snowflakes, we first examine the contribution F_L of liquid water flux to precipitation intensity, since it is an important input parameter for hydrological models. In Fig. 8a, the observed values of F_L are shown as colored circles. As shown, F_L tends to be high at higher temperatures, and the variation of F_L is somewhat complex around 0°C.

It is considered that the variation of F_L is strongly dependent on the vertical profiles of temperature and relative humidity aloft. In particular, when a refreezing layer exists, even a slight fluctuation in the temperature profile significantly affects the type of precipitation (Thériault et al. 2010). Sounding data measured at short time intervals cannot be obtained to explain the temporal variation of F_L, which sometimes drastically changed within a period of 10 min during our observations. Therefore, meteorological surface data were used to examine their relationship with F_L. Here, we assume the linear relationship between F_L, T (°C), RH (%), and R (mm h^{-1}) as

$$F_L = a_1 T + a_2 \mathrm{RH} + a_3 R + a_4, \tag{8}$$

where a_1, a_2, a_3 and a_4 are empirical constants, which were determined with the generalized reduced gradient (GRG) method (Lasdon et al. 1973) to minimize the RMSE between observed F_L and that estimated by (8). RMSE reached its minimum (0.160) when $a_1 = 0.371$, $a_2 = 0.0391$, $a_3 = -0.0668$, and $a_4 = -3.17$ (Fig. 8b). If the accuracy of the thermometer and humidity sensor is taken into account, the values of a_2 and a_4 fluctuate by values of ± 0.0003 and ± 0.1, respectively. Lines plotting (8) at $F_L = 1.0$ and $R = 1.0$ mm h^{-1} (red solid line) and at $F_L = 1.0$ and $R = 6.0$ mm h^{-1} (red dashed line) are shown in Fig. 8a. The values of F_L are dependent on R, since strong precipitation usually includes numerous large snowflakes, which take longer to melt. The empirical boundary between rain and melting snow proposed by Matsuo et al. (1981) (black dashed line) is between the two red lines, which suggests that (8) is consistent with the empirical boundary of this previous study. On the other hand, the lines of (8) at $F_L = 0.1$ and $R = 1$ mm h^{-1} (blue solid line) and at $F_L = 0.1$ and $R = 6$ mm h^{-1} (blue dashed line) are to the left of the empirical boundary between melting snow and snow (black solid line). Since Matsuo et al. (1981) utilized data that were based on visual observations, snowfall that included small amounts of liquid water may have been classified as "snow" in their study.

Note that (8) is a linear regression that is based on the observation data and is thus used within the observation ranges of the data. Histograms of T, RH, R, and F_L for the 44 observed cases are shown in Fig. 9. The values of T range from 0.1° to 1.79°C; data below 0.1°C were not obtained in this study, however (Fig. 9a). Therefore, (8) can be expected to produce large errors when it is applied to a case with $T < 0.1$°C, because F_L is considered to rapidly approach zero around $T = 0$°C and (8) does not guarantee $F_L = 0$ at $T = 0$°C. The observation range of RH is from 79.5% to 97.9%, but the majority of the data are greater than 90% (Fig. 9b). This suggests that the reliability of (8) is not high when RH < 90%. The ranges of R and F_L are from 0.06 to 6.45 mm h^{-1} and from 0.08 to 0.99, respectively (Figs. 9c and 9d).

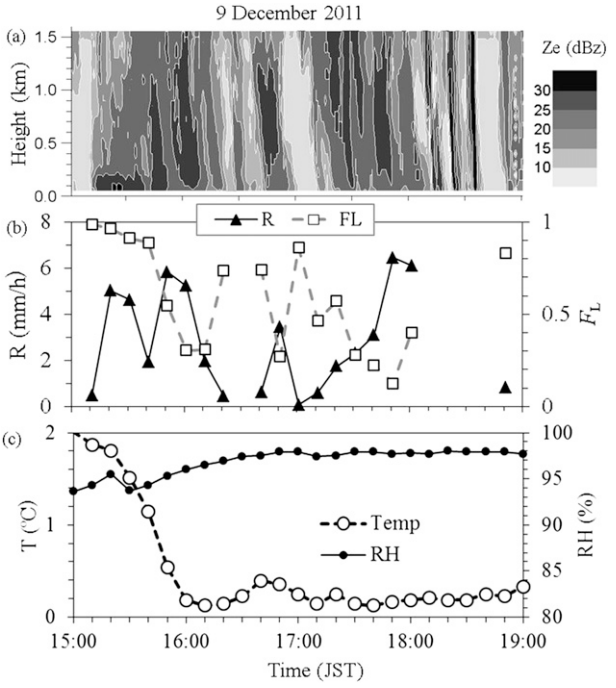

FIG. 7. As in Fig. 6, but from 1500 to 1900 JST 9 Dec 2011.

Figure 10 shows the averaged size spectra of the precipitation particles according to the classification of F_L (solid lines with white circles). The vertical axis N_h (cm^{-3} s^{-1}) is the number of particles per unit size interval that fall on a filter paper of a unit area during a unit of time (Ohtake 1969), represented as

$$N_h = V_t N(D), \tag{9}$$

where D is the melted diameter, V_t is the fall velocity of the particle with diameter D, and $N(D)dD$ is the number of particles per unit volume between D and $D + dD$. The gray lines in Fig. 10 indicate the empirical size distribution of snowflakes proposed by Gunn and Marshall (1958), where $V_t = 200D^{0.31}$ was assumed to be in cgs units. For all F_L classes, the observed size

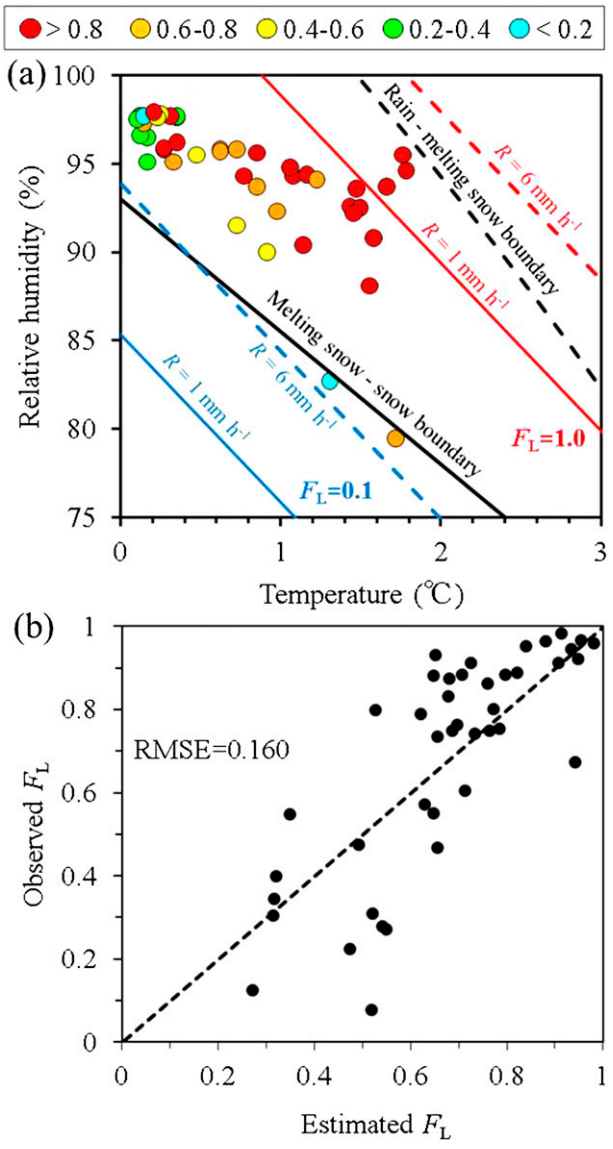

FIG. 8. (a) Temperature and relative humidity when the melting snowflakes were sampled (circles). The contributions of liquid water flux to precipitation intensity ($F_L = R_L/R$) are indicated by colored circles. The black solid and dashed lines are the empirical boundaries between snow and melting snow and between rain and melting snow, respectively, observed at Wajima, Japan, as provided by Matsuo et al. (1981). The blue solid, blue dashed, red solid, and red dashed lines represent the lines of (8) at $F_L = 0.1$ and $R = 1\,\mathrm{mm\,h^{-1}}$, $F_L = 0.1$ and $R = 6\,\mathrm{mm\,h^{-1}}$, $F_L = 1.0$ and $R = 1\,\mathrm{mm\,h^{-1}}$, and $F_L = 1.0$ and $R = 6\,\mathrm{mm\,h^{-1}}$, respectively. (b) Comparison of the F_L values estimated by (8) with the observed values.

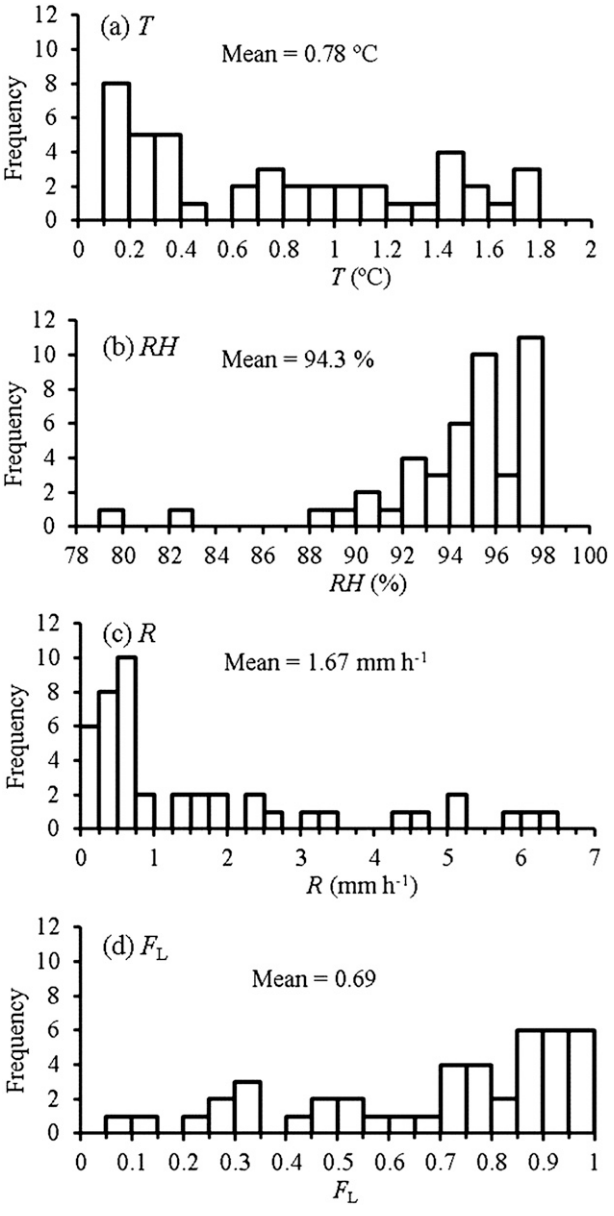

FIG. 9. Histograms of (a) T, (b) RH, (c) liquid-equivalent precipitation intensity R, and (d) F_L. Mean values are denoted above each figure.

distribution is close to the Gunn–Marshall distribution. The number of particles at $D > 3$ mm is fewer than that of the Gunn–Marshall distribution when $F_L > 0.4$, however. This result implies the occurrence of the breakup of snowflakes as a result of melting (Knight 1979; Fujiyoshi and Muramoto 1996), but a physical interpretation of the size distribution is difficult to obtain from these data alone. The maximum size of the observed particles is ~4 mm. We believe that the lack of snowflakes with $D >$ 4 mm is not caused by truncation due to the limited area of the filter papers, since Gunn and Marshall (1958) also did not observe particles with a diameter larger than 4 mm.

In Fig. 10, the size spectra of raindrops (dashed lines with filled circles) and snowflakes (dashed lines with plus signs) are also shown. As F_L increases, the number of small raindrops increases. Snowflakes with $D < 1$ mm still exist even when $0.8 \leq F_L < 1.0$, however (Fig. 10e).

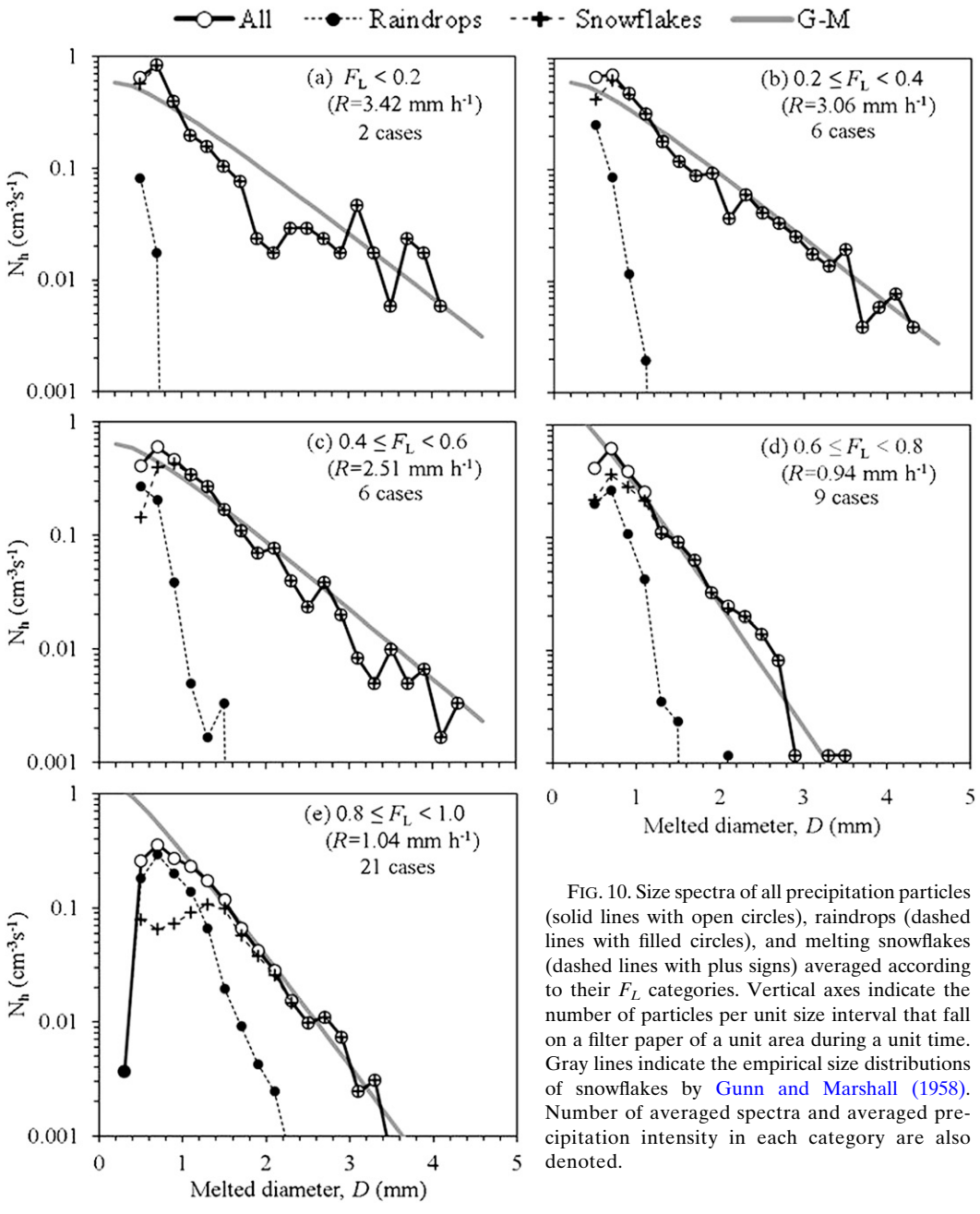

FIG. 10. Size spectra of all precipitation particles (solid lines with open circles), raindrops (dashed lines with filled circles), and melting snowflakes (dashed lines with plus signs) averaged according to their F_L categories. Vertical axes indicate the number of particles per unit size interval that fall on a filter paper of a unit area during a unit time. Gray lines indicate the empirical size distributions of snowflakes by Gunn and Marshall (1958). Number of averaged spectra and averaged precipitation intensity in each category are also denoted.

Precipitation particles observed in this study were a mixture of melting snowflakes and raindrops. The contribution F_R of raindrop flux to the total precipitation intensity is also important information because snowflakes and raindrops are usually treated separately in cloud-resolving models and simulations of radar scattering. The F_R was always below 0.1 when $F_L < 0.6$, and it rapidly increased when F_L exceeded 0.8 (Fig. 11). To represent such characteristics of F_R, the following fitting function was applied:

$$F_R = F_L \exp(b_1 F_L^3 + b_2 F_L^2 + b_3 F_L + b_4). \quad (10)$$

Under the constraint that $F_R = 1.0$ at $F_L = 1.0$, the coefficients were obtained by the GRG method as $b_1 = 16.3$, $b_2 = -20.3$, $b_3 = 8.4$, and $b_4 = -4.4$ with the coefficient of determination r^2 equal to 0.77 (solid curve in Fig. 11). The gradient of F_R in (10) becomes large as F_L approaches 1.0. Therefore, the accuracy of F_L is also important when (10) is used for large F_L, since the errors in F_L could affect the estimation of F_R because of the large gradient of F_R.

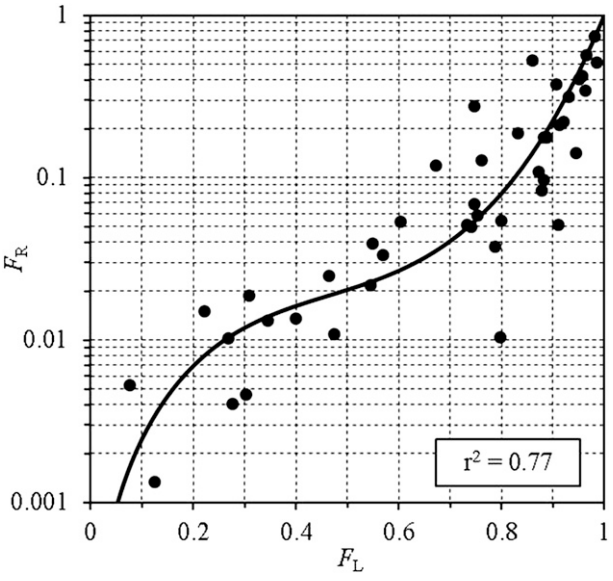

FIG. 11. Relationship between F_L and F_R. The solid curve indicates the best-fit line represented by (10). The coefficient of determination is indicated by r^2.

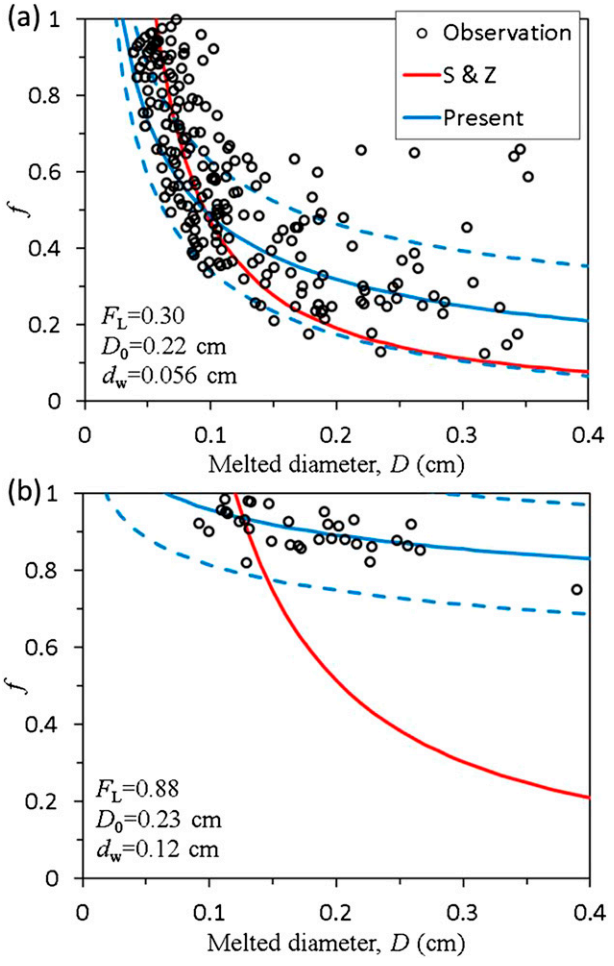

FIG. 12. Relationship between f and melted diameter at (a) 1601 JST 9 Dec and (b) 0330 JST 26 Mar 2011. Small circles are the observed values. The solid and dashed blue lines are the curves of (17) and the boundaries of the RMSE (=0.144), respectively. The red lines indicate the relationship proposed by Szyrmer and Zawadzki (1999).

c. *Liquid water fraction of individual snowflakes*

Figure 12 shows the relationship between D and f of snowflakes observed at 1601 JST 9 December 2011 and at 0330 JST 26 March 2011. Values of f decrease as D increases. The same tendency was pointed out by Nakamura (1960) and Sasyo et al. (1991) in their observation of melting snowflakes. The values of f are also dependent on F_L; the decreasing rate of f with D is smaller for large values of F_L (Fig. 12b). Here, the size dependence of f will be empirically expressed as follows:

$$f = \alpha(D/D_0)^{-\beta}, \tag{11}$$

where D_0 is the median mass diameter of the snowflakes at each observation and α and β are the empirical parameters that are dependent on F_L. By normalizing D by D_0, the effects of the slope parameter on the particle size distribution can be eliminated (Sekhon and Srivastava 1970). In the derivation of D_0, the data for raindrops are excluded and only the data for melting snowflakes are used.

To obtain D_0, it is convenient to fit the size distributions of snowflakes with a distribution function. According to Fig. 10, the size distribution of snowflakes is close to that of Gunn and Marshall (1958) when F_L is small, and it gradually changes to a concave downward form as F_L increases, which could be fitted by a gamma distribution given as follows:

$$N(D) = N_0 D^{\mu} \exp(-\Lambda D), \tag{12}$$

where N_0, μ, and Λ are parameters. When the size distribution of the snowflakes is obtained with (12), D_0 is related to the mass-weighted mean diameter D_m as (Ulbrich 1983)

$$D_m = \frac{\int_0^{\infty} D^4 N(D)\, dD}{\int_0^{\infty} D^3 N(D)\, dD} = \left(\frac{4+\mu}{3.67+\mu}\right) D_0. \tag{13}$$

Because the value of μ does not have a large impact on the relation (13) when $\mu \geq -2$ (Ulbrich 1983), we assumed $\mu = 0$ in our study. Diameter D_m was estimated from the number, size, and fall velocity of particles as

$$D_m = \frac{\sum_{i=1}^{n}\left(\frac{N_i D_i^4}{V_{ti} A \Delta t}\right)}{\sum_{i=1}^{n}\left(\frac{N_i D_i^3}{V_{ti} A \Delta t}\right)}, \quad (14)$$

where N_i and V_{ti} are the number and fall velocity of snowflakes with melted diameter D_i, A is the area of a filter paper, and Δt is the exposure time of filter paper. The summation in (14) was carried out over n diameter classes. The fall velocity of melting snowflakes V_{ti} was not observed in this study; therefore, the fall velocity was calculated by the method given by Szyrmer and Zawadzki (1999), in which fall velocity is a function of both D and f. Once D_m is obtained, D_0 can be calculated using (13).

After D_0 was determined, (11) was fitted to the observed f, and the values of α and β were obtained for each observation time. To fit (11) to the observed f, only data for melting snowflakes ($f < 1.0$) were used. Figure 13 shows four examples of such fittings. According to the r^2 values, (11) fits the data fairly well, although the data are scattered around the fitting line in some cases. The values of α, which are equal to the values of f at $D/D_0 = 1$, increase with F_L, whereas the values of β decrease with F_L. Figure 14 shows the relationships between α and F_L and between β and F_L. With $r^2 = 0.97$ (Fig. 14a), the variations in α were approximated by a linear function of F_L that passes through the origin, such as follows:

$$\alpha = F_L. \quad (15)$$

With $r^2 = 0.91$ (Fig. 14b), the variations in β can be well explained by a linear function of F_L:

$$\beta = 0.86(1 - F_L). \quad (16)$$

By combining (11), (15), and (16), the empirical relationship for estimating f is obtained as

$$f = F_L (D/D_0)^{-0.86(1-F_L)}. \quad (17)$$

Equation (17) fulfills the requirement for f to become 0 at $F_L = 0$, and f becomes 1 at $F_L = 1$.

Figure 15 compares f estimated by (17) and the observed values for the 3632 snowflakes. The observed data here are not from independent datasets, but they are the same data that were used to derive (17). The plot is somewhat scattered (RMSE = 0.144), but the data are well correlated considering the number of samples (correlation coefficient: 0.77). If the F_L values estimated by (8) are used in place of the observed values, the RMSE of (17) increases to 0.190 (figure not shown). Equation (17) was also applied to the two examples shown in Fig. 12 (blue lines). In these two cases, 58.8% (Fig. 12a) and 100% (Fig. 12b) of the observed f values are within the RMSE boundaries of (17) (dashed blue lines).

4. Discussion

a. Measurement errors

In this study, an empirical relationship for estimating f was proposed on the basis of filter-paper observations [see (17)], but the values of f are scattered around the empirical lines (Fig. 15). There are two possible causes for the dispersion, one of which is the natural variability of the melting snowflakes. Yuter et al. (2006) showed that the standard deviation for the fall speed of wet snow was larger than that of dry snow. This suggests that f may vary for snowflakes even when their melted diameters are identical under the same conditions, because of the variability of their shape and trajectories. Another possible cause for the dispersion is measurement errors. In this section, we will evaluate the effects of measurement errors and natural variability.

First, we assume that the errors associated with the conversion from spotted area to water mass (standard deviation of relative error: 6.6%) and the calibration errors (RMSE = 0.108) have a Gaussian distribution near the ''true values.'' Although the calibration errors may have a bias, such an effect is not taken into account here, since it cannot be evaluated. The true values of M_1 and M_2 in (3) for the 3632 observed snowflakes were virtually produced by subtracting the errors generated by the Gaussian random number generator. Then, f_1 was calculated using (3) and was converted to f using (4). Next, the true values of f were obtained by subtracting errors generated from the Gaussian random number generator. The RMSE between the true values of f and observed f was 0.110. This is the estimated value for the measurement error of f. The measurement error for F_L was evaluated using the same method. The standard deviation of the measurement errors of F_L for 44 observations was 0.0248. The relatively small error for F_L was due to the fact that the errors in the mass of individual snowflakes offset each other when they are summed to calculate rainfall intensity.

The RMSE between observed f and the fitted line was 0.144 (Fig. 15). If the RMSE is assumed to be the root of the sum of the variances that are due to the measurement error and that due to natural variability, the RMSE of f that is due to the natural variability is estimated to be 0.0929.

b. Comparison with previous studies

We measured the liquid water fraction of snowflakes using the same technique as Sasyo et al. (1991). They expressed the liquid water fraction of a snowflake as

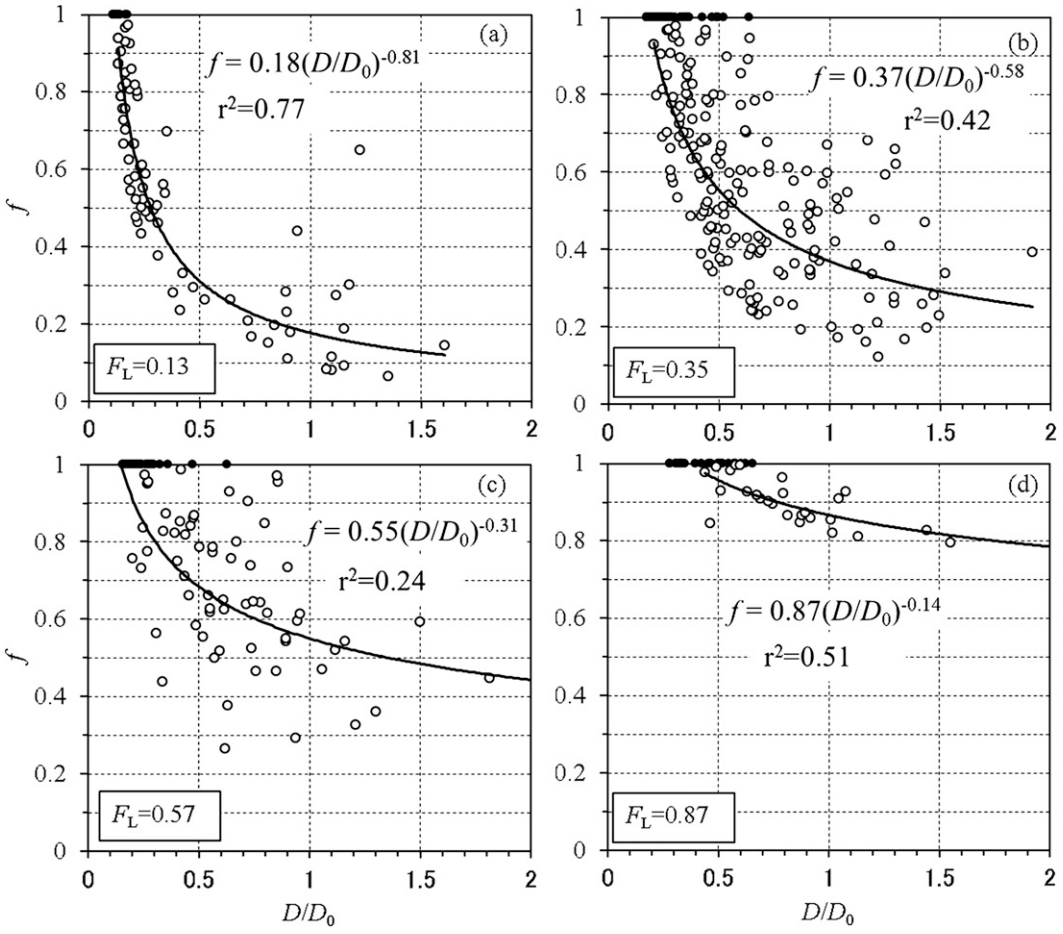

FIG. 13. Four examples of relationships between D/D_0 and f of snowflakes (open circles) for different F_L observed at (a) 1751 JST 9 Dec, (b) 1845 JST 24 Dec, (c) 1721 JST 9 Dec, and (d) 0410 JST 26 Mar 2011. Solid lines indicate the best-fit curves, and the coefficient of determination is denoted by r^2. Filled circles indicate the raindrops that were not used to derive the best-fit lines.

$$f = c_1 M_s^{-c_2}, \tag{18}$$

where M_s is the mass of a snowflake and c_1 and c_2 are empirical constants. To compare (18) with (17), the following is substituted into (18):

$$M_s = (\pi\rho_w/6)D^3. \tag{19}$$

This procedure produces the following:

$$f = c_1(\pi\rho_w/6)^{-c_2} D^{-3c_2}, \tag{20}$$

where ρ_w is the density of water. By comparing (20) with (17), c_2 can be expressed as

$$3c_2 = 0.86(1 - F_L). \tag{21}$$

In (21), c_2 should change from 0 to 0.287 when F_L varies from 1.0 to 0. However, the range of c_2 was from 0.27 to 0.95 in Sasyo et al. (1991). This discrepancy can be explained by the effects of our calibration. If f is corrected in (20) by using (4), the following can be obtained:

$$f = c_1^{0.403}(\pi\rho_w/6)^{-0.403c_2} D^{-1.21c_2}. \tag{22}$$

By comparing (22) with (17), c_2 can be expressed as

$$1.21c_2 = 0.86(1 - F_L). \tag{23}$$

In (23), c_2 changes from 0 to 0.71 when F_L varies from 1.0 to 0. This range overlaps with that of Sasyo et al. (1991) (from 0.27 to 0.95). The difference between the upper limits of c_2 is probably due to the type of the precipitation particle; they obtained c_2 = 0.95 for heavily rimed crystals or graupel, which were not investigated in our study. The difference between the lower limits is due to their observation range; that is, they observed only six cases.

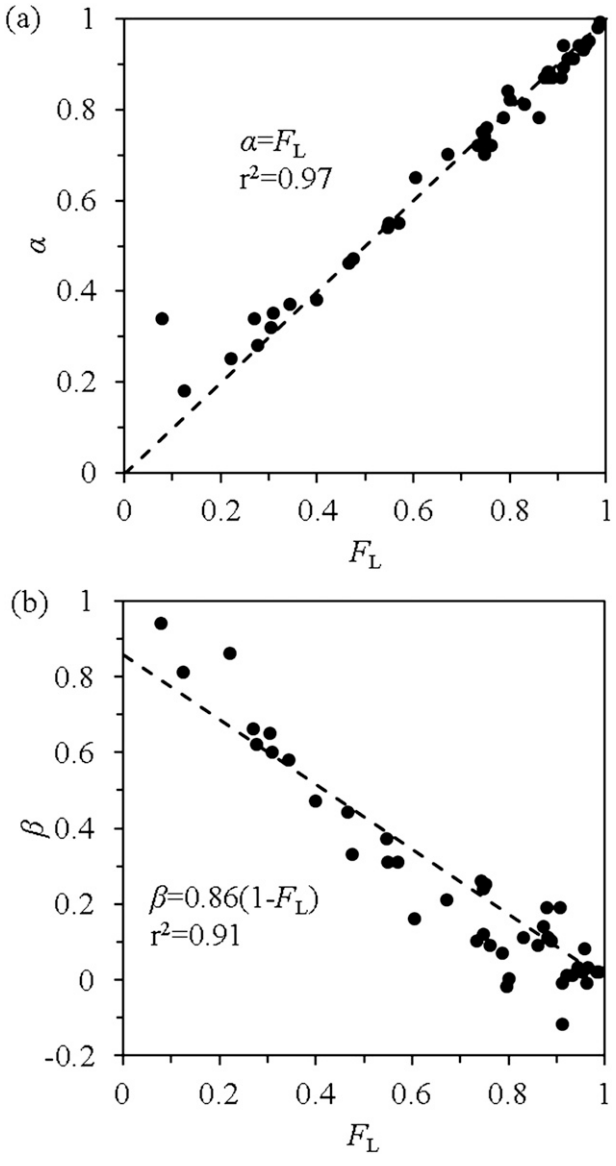

FIG. 14. Relationship between (a) α and F_L and (b) β and F_L. Dashed lines indicate linear approximations, and the coefficient of determination is denoted by r^2.

For c_1, the following relationship can be obtained by comparing (17) with (22):

$$c_1 = F_L^{2.48}\left(\frac{\pi\rho_w}{6}D_0^3\right)^{0.711(1-F_L)}. \quad (24)$$

In (24), the range of c_1 is from 0 to 1 when $D_0 < 3$ mm and $\rho_w = 1.0\,\mathrm{g\,mm^{-3}}$, which covers the range of c_1 in Sasyo et al. (1991) (from 0.07 to 0.51). In summary, the difference in the empirical relationship of our study and that of Sasyo et al. (1991) can be attributed to the inclusion of a calibration, differences in the observation range, and the type of precipitation particles.

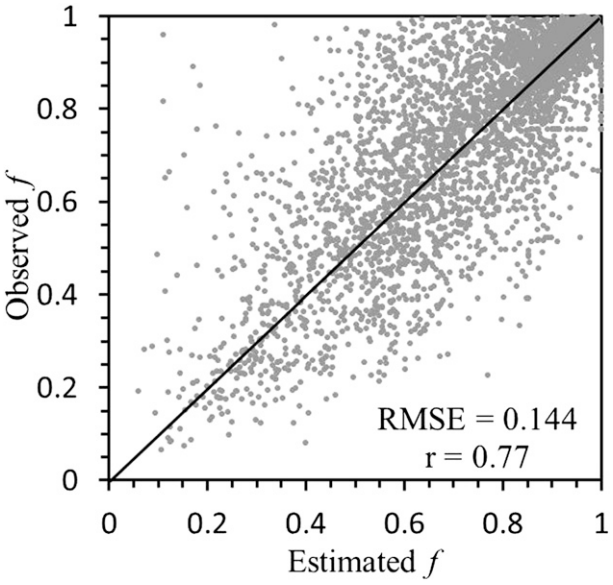

FIG. 15. Scatterplot of f estimated by (17) vs the observed values; r indicates the correlation coefficient.

Szyrmer and Zawadzki (1999) formulated f on the basis of their theoretical consideration as

$$f = (D/d_w)^{-1.3}, \quad (25)$$

where d_w is defined as the melted diameter of melting snow when it is entirely covered with liquid water. They approximated d_w as the diameter such that $f(d_w) = 1.0$ to derive (25). A direct comparison of (25) with the formulation of f in our study is difficult, because d_w cannot be defined as a unique value in our data. Szyrmer and Zawadzki (1999) assumed that d_w is the diameter that separates wet snow from rain. As shown in Fig. 10, however, the raindrops and snowflakes observed in our study coexisted in the same range of melted diameter. Thus, for convenience, d_w is calculated as the average of the maximum diameter of raindrops (particles with $f = 1.0$) and the minimum diameter of snowflakes (particles with $f < 1.0$) to apply (25) to our observation data (red lines in Fig. 12). The curve of (25) is similar to that of (17) when $F_L = 0.30$ (Fig. 12a), whereas it significantly underestimates f for large particles when $F_L = 0.88$ (Fig. 12b). The difference between (25) and (17) is attributed to the exponent on the right-hand side, which is a constant value in (25) but changes from -0.86 to 0 in (17), depending on the values of F_L. Szyrmer and Zawadzki (1999) obtained (25) by assuming that a population of melting snowflakes experiences the same time period for

melting, since their purpose was to construct a bulk microphysics module for a melting layer. On the other hand, the snowflakes observed in this study could have fallen through different trajectories before reaching a filter paper and would have then experienced a variety of melting periods and atmospheric conditions. This scenario is considered to be the cause of the difference between (25) and (17).

5. Summary

A ground-based observation of the liquid water fraction of snowflakes was carried out in Nagaoka using dye-treated filter papers kept at 0°C. Data were calibrated on the basis of an experiment using imitation snowflakes. The RMSE of the measurement of f was estimated to be 0.110. As a result, we obtained an empirical relationship between the contribution F_L of liquid water flux to precipitation intensity and meteorological surface data [(8)] and a relationship for estimating the liquid water fraction of individual snowflakes as a function of melted diameter, median mass diameter, and F_L [(17)]. It was determined that the RMSEs for estimating F_L and f by using these relationships were 0.160 and 0.144, respectively. The ratio F_R of raindrop flux to precipitation intensity was always below 0.1 when $F_L < 0.6$ but increased rapidly when F_L exceeded 0.8. The empirical relationship to estimate F_R using F_L was obtained as (10), with RMSE = 0.110.

The empirical relationships obtained in this study were the regressions that are based on the observation data and have not been tested by using independent datasets. We need to examine the applicability of the relationships to other datasets, especially to data obtained in climatologically different places where ice crystal types differ from those at our observation site.

In a cloud-resolving model with a bulk microphysics scheme, F_L is easily obtained from the ratio between the liquid water precipitation rate and the total precipitation rate. Thus, the empirical relationship proposed in this study could be used to estimate the contribution of raindrop flux to the total precipitation intensity and the size dependence of the liquid water fraction of snowflakes in a cloud-resolving model, which are important parameters to calculate radar reflectivity in a melting layer. We are planning to investigate whether the use of the empirical relationships proposed in this study could improve the estimation of radar reflectivity using numerical model outputs.

Acknowledgments. The authors are grateful to the three anonymous reviewers for their kind and constructive comments. The authors also thank Suga Test Instrument Co., Ltd., for kindly providing the instrument used in this study.

REFERENCES

Austin, P. M., and A. C. Bemis, 1950: A quantitative study of the "bright band" in radar precipitation echoes. *J. Meteor.,* **7,** 145–151, doi:10.1175/1520-0469(1950)007<0145:AQSOTB>2.0.CO;2.

Fujiyoshi, Y., 1986: Melting snowflakes. *J. Atmos. Sci.,* **43,** 307–311, doi:10.1175/1520-0469(1986)043<0307:MS>2.0.CO;2.

——, and K. Muramoto, 1996: The effect of breakup of melting snowflakes on the resulting size distribution of raindrops. *J. Meteor. Soc. Japan,* **74,** 343–353. [Available online at https://www.jstage.jst.go.jp/article/jmsj1965/74/3/74_3_343/_pdf.]

Gunn, K. L. S., and J. S. Marshall, 1958: The distribution with size of aggregate snowflakes. *J. Meteor.,* **15,** 452–461, doi:10.1175/1520-0469(1958)015<0452:TDWSOA>2.0.CO;2.

Ishizaka, M., 1995: Measurement of falling velocity of rimed snowflakes (in Japanese). *Seppyo,* **57,** 229–238. [Available online at https://www.jstage.jst.go.jp/article/seppyo1941/57/3/57_3_229/_pdf.]

Klaassen, W., 1988: Radar observations and simulation of the melting layer of precipitation. *J. Atmos. Sci.,* **45,** 3741–3753, doi:10.1175/1520-0469(1988)045<3741:ROASOT>2.0.CO;2.

Knight, C. A., 1979: Observation of the morphology of melting snow. *J. Atmos. Sci.,* **36,** 1123–1130. [Available online at http://journals.ametsoc.org/doi/abs/10.1175/1520-0469%281979%29036%3C1123%3AOOTMOM%3E2.0.CO%3B2.]

Lasdon, S. L., R. Fox, and M. Ratner, 1973: Nonlinear optimization using the generalized reduced gradient method. Case Western Reserve University Dept. of Operations Research Tech. Memo. 325, 63 pp. [Available online at http://www.dtic.mil/dtic/tr/fulltext/u2/774723.pdf.]

Maahn, M., and P. Kollias, 2012: Improved Micro Rain Radar snow measurements using Doppler spectra post-processing. *Atmos. Meas. Tech.,* **5,** 2661–2673, doi:10.5194/amt-5-2661-2012.

Matsuo, T., and Y. Sasyo, 1981: Empirical formula for the melting rate of snowflakes. *J. Meteor. Soc. Japan,* **59,** 1–9. [Available online at https://www.jstage.jst.go.jp/article/jmsj1965/59/1/59_1_1/_pdf.]

——, ——, and Y. Sato, 1981: Relationship between types of precipitation on the ground and surface meteorological elements. *J. Meteor. Soc. Japan,* **59,** 462–476. [Available online at https://www.jstage.jst.go.jp/article/jmsj1965/59/4/59_462/_pdf.]

Mitra, S. K., O. Vohl, M. Ahr, and H. R. Pruppacher, 1990: A wind tunnel and theoretical study of the melting behavior of atmospheric ice particles. IV: Experiment and theory for snow flakes. *J. Atmos. Sci.,* **47,** 584–591, doi:10.1175/1520-0469(1990)047<0584:AWTATS>2.0.CO;2.

Nakamura, T., 1960: On the method measuring the liquid water content of falling snowflakes (in Japanese). *Seppyo,* **22,** 145–146, doi:10.5331/seppyo.22.145.

Ohtake, T., 1969: Observations of size distributions of hydrometeors through the melting layer. *J. Atmos. Sci.,* **26,** 545–557, doi:10.1175/1520-0469(1969)026<0545:OOSDOH>2.0.CO;2.

Oraltay, R. G., and J. Hallett, 1989: Evaporation and melting of ice crystals: A laboratory study. *Atmos. Res.,* **24,** 169–189, doi:10.1016/0169-8095(89)90044-6.

——, and ——, 2005: The melting layer: A laboratory investigation of ice particle melt and evaporation near 0°C. *J. Appl. Meteor.,* **44,** 206–220, doi:10.1175/JAM2194.1.

Sasyo, Y., T. Mori, O. Onozaki, and T. Saito, 1991: Observation of the liquid water content of melting snowflakes with a new

instrument. *J. Meteor. Soc. Japan,* **69,** 83–90. [Available online at https://www.jstage.jst.go.jp/article/jmsj1965/69/1/69_1_83/_pdf.]

Sekhon, R. S., and R. C. Srivastava, 1970: Snow size spectra and radar reflectivity. *J. Atmos. Sci.,* **27,** 299–307, doi:10.1175/1520-0469(1970)027<0299:SSSARR>2.0.CO;2.

Szyrmer, W., and I. Zawadzki, 1999: Modeling of the melting layer. Part I: Dynamics and microphysics. *J. Atmos. Sci.,* **56,** 3573–3592, doi:10.1175/1520-0469(1999)056<3573:MOTMLP>2.0.CO;2.

Thériault, J. M., R. E. Stewart, and W. Henson, 2010: On the dependence of winter precipitation types on temperature, precipitation rate, and associated features. *J. Appl. Meteor. Climatol.,* **49,** 1429–1442, doi:10.1175/2010JAMC2321.1.

Ulbrich, C. W., 1983: Natural variation in the analytical form of the raindrop size distribution. *J. Climate Appl. Meteor.,* **22,** 1764–1775, doi:10.1175/1520-0450(1983)022<1764:NVITAF>2.0.CO;2.

Yamaguchi, S., K. Iwamoto, and S. Nakai, 2013: Interannual fluctuations of the relationship between winter precipitation and air temperature in the heavy-snowfall zone of Japan. *Ann. Glaciol.,* **54,** 183–188, doi:10.3189/2013AoG62A302.

Yuter, S. E., D. E. Kingsmill, L. B. Nance, and M. Löffler-Mang, 2006: Observation of precipitation size and fall speed characteristics within coexisting rain and wet snow. *J. Appl. Meteor. Climatol.,* **45,** 1450–1464, doi:10.1175/JAM2406.1.

Zawadzki, I., W. Szyrmer, C. Bell, and F. Fabry, 2005: Modeling of the melting layer. Part III: The density effect. *J. Atmos. Sci.,* **62,** 3705–3723, doi:10.1175/JAS3563.1.